Formation and consequences of misfit dislocations in heteroepitaxial growth

MARKUS WALTHER[1], MICHAEL BIEHL[2], WOLFGANG KINZEL[1]

[1] Institut für Theoretische Physik und Astrophysik
Julius-Maximilians-Universität Würzburg
Am Hubland, 97074 Würzburg, Germany

[2] Institute of Mathematics and Computing Science
University of Groningen, P.O. Box 800
9700 AV Groningen, The Netherlands

May 23, 2007

Abstract

We investigate the formation of misfit dislocations in strained heteroepitaxial crystal growth and their influence on the structure of the growing layers. We use Kinetic Monte Carlo simulations for an off-lattice model in 1+1 dimensions with Lennard-Jones interactions. Two different types of the formation of dislocations are found, depending on the sign and the magnitude of the misfit. Misfit dislocations affect the lateral and the vertical lattice spacing in heteroepitaxial growth. In addition, we observe a correlation between the lateral position of buried dislocations and grown mounds, depending on the sign of the misfit.

1 Introduction

Due to its high technological relevance, epitaxial growth of semiconductor interfaces has become a field of intensive study in the past years. From a theoretical point of view, epitaxial growth is an example of cooperative behavior far from thermal equilibrium which is still an active field of research. Epitaxial layers of atoms and molecules can be realized by molecular beam epitaxy which allows to design high quality semiconductor structures on an atomic scale. In the case of heteroepitaxy, substrate and adsorbate consist of different materials and may differ in their lattice constants. This leads to interesting structures of the growing atomic layers. The first few adsorbate layers can grow pseudomorphically, i.e. coherently with the crystal structure of the substrate. But due to strain the elastic energy of the system rises with increasing adsorbate film thickness. At a critical layer thickness the strain is released by forming misfit dislocations.

In this work the detailed mechanisms of the formation of dislocations are investigated with means of Kinetic Monte Carlo Simulations [1, 2, 3]. It is obvious that dislocations cannot be modelled properly with predefined lattice structures, hence we use an off-lattice model. Since we are interested in the general phenomenon of epitaxial growth competing with strain and dislocations, we use Lennard-Jones interactions. As a starting point, we investigate (1+1)-dimensional models with classical pair-interactions and lateral extensions of a few hundred lattice spacings. Even in this fairly limited framework we observe complex phenomena which can be compared with experiments and yield qualitative insights into heteroepitaxial growth. Following previous studies [3, 4, 5, 6], we choose a pair potential to model the interactions between substrate and adsorbate particles and we apply

an off-lattice algorithm to the simulation of the growth of heteroepitaxial layers in 1+1 dimensions.

We have investigated the formation of dislocations as well as their influence on the vertical and the lateral lattice spacings. In addition, we found that buried dislocations have a pronounced influence on the surface structure of the subsequent growth.
Our model does not aim at describing a concrete material system, we rather address general aspects and qualitative features of heteroepitaxial growth. The essential mechanisms then can be realized with a small set of parameters and give insight to strain related processes. Nevertheless it is possible to extend the model and include more specific details. The method used for simulations of heteroepitaxial growth in 1+1 dimensions was introduced in [1, 2, 3].

2 Model and method

In order to simulate heteroepitaxial growth, we use an off-lattice model where the particles have continuous coordinates in space, as introduced and discussed in [1, 2, 7]. Since we are interested in general features of heteroepitaxial growth we model the interactions between the particles by a Lennard-Jones potential of the form

$$U_{ij}(U_0, \sigma) \;=\; 4\, U_0 \left[\left(\frac{\sigma}{r_{ij}} \right)^{12} - \left(\frac{\sigma}{r_{ij}} \right)^{6} \right]. \tag{1}$$

The attractive contribution in the potential competes with the strong repulsive part dominating at small distances. While the exponent 6 of the attractive part is motivated by van der Waals dispersion forces, originated by dipole-dipole interactions in turn due to fluctuating dipoles, the exponent 12 is chosen exclusively for practical reasons as it allows to calculate the potential energy very efficiently. The parameters U_0 and σ specify the different material properties in the model. The interaction of two substrate particles is given by $U_{ij}(U_s, \sigma_s)$ and accordingly for two adsorbate particles by $U_{ij}(U_a, \sigma_a)$. To keep the number of parameters small, we follow a standard approach and set the interaction between substrate and adsorbate particles to $U_{ij}\left(\sqrt{U_a U_s}, (\sigma_s + \sigma_a)/2\right)$.

In the following simulations we set $U_s = U_{as} = U_a$ which allows to isolate the influence of the misfit from energetic effects. To set the energy scale, the potential depth in the simulation is $U_0 = 1.3125\, eV$ which leads to a diffusion barrier of about $0.90\, eV$ for an isolated adsorbate particle on a plane substrate surface. Since the interaction strength decreases fast with the particle distance, a cut-off distance r_{cut} with $U_{ij} = 0$ for $r_{ij} > r_{cut}$ is assumed. The cut-off is chosen to be $r_{cut} = 3\, r_0$, because in this case the value of the potential is already less than one percent of the equilibrium distance $r_0 = 2^{\frac{1}{6}}\, \sigma$ of two isolated adatoms. This cut-off is necessary since the computer time required for calculating the energy increases with the number of involved particles.

The lattice spacing is proportional to σ and therefore the relative lattice mismatch can be described by the relation

$$\epsilon = \frac{\sigma_a - \sigma_s}{\sigma_s}. \tag{2}$$

In our simulation adsorbate particles are deposited randomly on a one-dimensional substrate surface with a constant and homogeneous particle flux F. The relevant parameter is the deposition rate $R_d = L\, F$. We include a mechanism where the kinetic energy enables deposited particles arriving at the surface to slide down to the lowest position locally available. This so called "downhill funneling" and similar incorporation mechanisms which smoothen the surface morphology are discussed in [8]. We assume periodic boundary conditions in lateral direction and fix particle positions of the three bottom substrate layers to

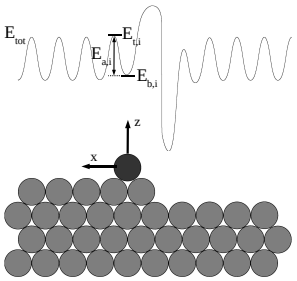

Figure 1: Potential energy surface of an adatom. See text for further information.

stabilize the crystal. We only consider jumps of particles to the next left or right neighboring minimum in the potential energy surface. The rate R_i for the thermally activated diffusion process is given by an Arrhenius law:

$$R_i = \nu_0 \, e^{-\frac{E_{a,i}}{k_B T}}. \tag{3}$$

Here T is the simulation temperature, k_B the Boltzmann constant and ν_0 the attempt frequency. For simplification, for all processes the attempt frequency is set to the constant value $\nu_0 = 10^{12} s^{-1}$. The activation energy $E_{a,i}$ for the diffusion step i is given by the difference between the system energy at the bindings state $E_{b,i}$ and the transition state $E_{t,i}$ as displayed in Figure 1. The total potential energy of a system consisting of n particles is

$$E_{tot} = \sum_{i=1}^{n} \sum_{j=i+1}^{n} U_{ij}. \tag{4}$$

To calculate the activation energies precisely, it is indispensable to determine the transition energy by considering the relaxation of the neighboring particles. An approved and robust method is the so called "Activation Relaxation Technique", introduced in [9]. The dynamics then is realized by choosing one event j with the rate R_j according to its probability $p_j = R_j / (R_d + \Sigma_i R_i)$. This combination of KMC simulations with Molecular Static evaluation of barriers was introduced by D. Wolf and collaborators [10] in the context of strain induced dislocations. The potential energy surface shown in Figure 1 is calculated by moving the black adatom virtually in the x-direction. The total energy is minimized by variation the z coordinate of this adatom and the coordinates of all other particles.

As an important simplification we apply the so-called frozen crystal approximation when evaluating transition state energies. Thereby, the position of all particles except for the diffusing adatom are considered constant in the Molecular Static procedure. Clearly this restricts the accuracy of the method. However, we find that barriers calculated within the frozen crystal approximation differ typically less than 10% from the correct ones in our model.

Due to the high binding energies, the desorption rates are very small compared to the rates of deposition and diffusion. Therefore desorption is disregarded in the simulation, as well as exchange diffusion and multiple jumps.

After a microscopic event performed within the frozen crystal approximation, the configuration of the crystal does not correspond precisely to a local minimum of the total energy. In order to compensate for this effect and incorporate the deformation of the crystal correctly, the energy (4) is minimized after each event by means of a conjugate gradient method [11]. In order to speed up the simulations, this relaxation is performed only locally after each event, while global relaxation is applied after a larger number of simulation steps. In the former, the minimization is only with respect to particle positions closer to the diffusing or deposited adatom than the cut-off distance. Global relaxation affects the entire

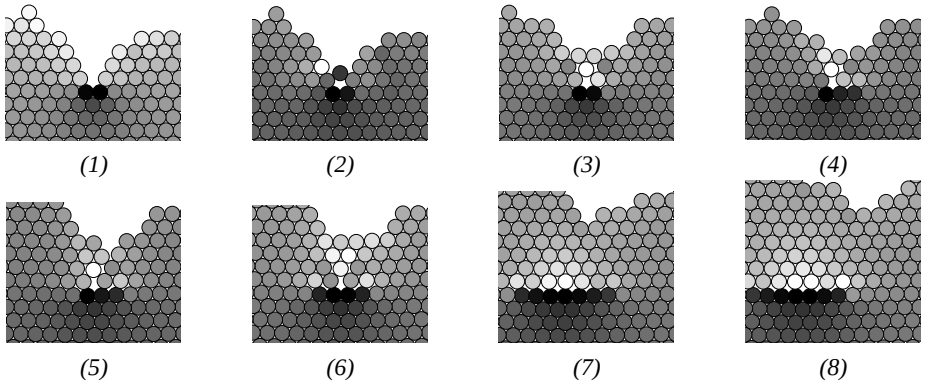

Figure 2: The formation of a dislocation simulated with a positive misfit $\epsilon = +3.0\%$. This sequence of snapshots shows the evolution of a section of a larger system. The grey level of a particle indicates the average distance to its nearest neighbors. The lighter a particle is drawn, the larger is this distance.

system. Note that the relaxation procedures only take the energy of the system to its nearest local minimum. This is achieved by small changes of the particle positions only, without changing the crystal topology. Nevertheless, all diffusion barriers have to be recalculated and the resulting rates have to be updated.

3 Strain relaxation mechanism: misfit dislocation

3.1 Formation of dislocations

In heteroepitaxial growth, the substrate and the adsorbate material differ in the lattice constant. For moderate values of the misfit ($|\epsilon| \ll 1$) the adsorbate first grows coherently with the substrate. In this pseudomorphic phase the substrate determines the lateral lattice constant of the adsorbate. As a consequence the strain energy stored in the growing film increases. Far away from the substrate, one expects that the substrate has no significant influence on the adsorbate and the adsorbate can grow with its own lattice constant. As a result, the strain of the system can be released by the formation of a misfit dislocation at a critical adsorbate thickness, as it was observed in [1]. The thickness of a dislocation free adsorbate film mainly depends on the misfit of the adsorbate material, as well as on the potential depth of the substrate adsorbate interaction potential. In the following simulations the temperature is set to $T = 450\,K$ and the flux to $F = 1\,MLs^{-1}$.

For positive misfit less than $\epsilon \approx +3\%$ the adsorbate initially grows coherently with the substrate. The appearance of a dislocation does not only depend on the misfit between adsorbate and substrate and on details of the surface morphology, but also on the deposition rate and the substrate temperature. Details will be reported elsewhere. We conclude that dislocation formation is a kinetic process which cannot be understood by purely energetic arguments.

The mechanism of an evolving dislocation is shown in Figure 2. Due to the Ehrlich-Schwoebel effect the diffusing particles on top of islands tend to form mounds instead of growing layer by layer [12, 13]. At the critical adsorbate height the lateral distance between two neighboring mounds is not large enough to allow an additional particle between the mounds, as shown in the case (2). Hence the particle between the two mounds is dislocated from the supposed lattice position (2). This position is the seed of a dislocation which is overgrown by further adsorbate material, by both deposition and diffusion. The grey level of the particles just indicates the average distance of a particle to its neighbors. The lighter

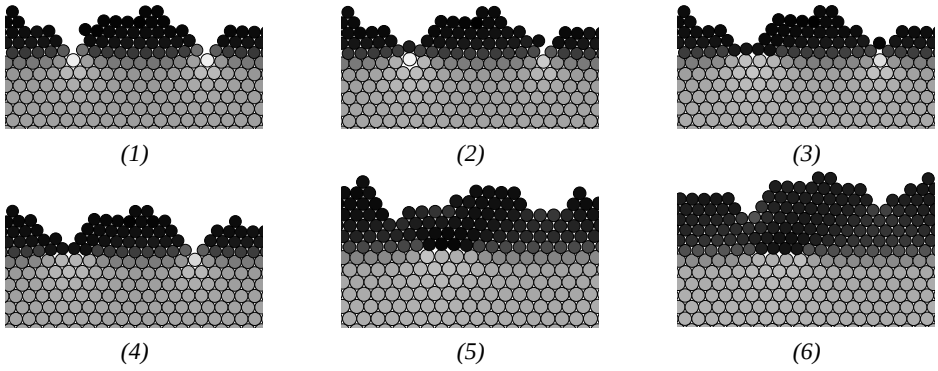

Figure 3: The formation of a dislocation simulated with a negative misfit $\epsilon = -11.0\%$. This sequence of snapshots shows the evolution of a section of a larger system. The grey level of a particle indicates the average distance to its nearest neighbors. The lighter a particle is drawn, the larger is this distance.

a particle is drawn, the larger is the average distance to its neighbors. As the exact particle distances may change when distorting the surface, also the grey value of a given particle changes during the simulation.

Above the critical adsorbate thickness several dislocations are formed in a range of just few monolayers in the whole system. Note that the formation of a dislocation is favored by the presence of mounds.

For higher values of positive misfit no pseudomorphic growth is observed and the dislocations are formed directly on the substrate very similar to the formation mechanism shown in Figure 2. The number of dislocations increases with the misfit and the mean distance between dislocations is close to $1/\epsilon$ which reflects the relative periodicity of the substrate and adsorbate lattice [13].

In the case of negative misfit a dislocation is formed by two different mechanisms. For high values of negative misfit, like $|\epsilon| \gtrsim 8\%$ the dislocations are formed directly on the substrate in analogy to the case of high positive misfit. This behavior is shown in Figure 3. Again, two neighboring mounds of adsorbate are seed for a new emerging dislocation. On panel (1) one can see a resulting gap between the two bottom edge particles of the adjacent mounds. This gap enables the diffusing particle on the slope of the right mound to move in between, as displayed in panel (2). The following panels document the overgrowing of this dislocation by further adsorbate material.

For lower values of negative misfit, like $|\epsilon| \lesssim 6\%$ the adsorbate first grows coherently with the substrate until a dislocation appears to release the strain. But here, the mechanism of the formation is different, as it can be seen in Figure 4. In contrast to the case of positive misfit the mean adsorbate particle distance is increased in the pseudomorphic growth compared to its own lattice constant. Therefore, the adsorbate particles can react more flexibly on changes in the surface topology without reaching the strong repulsive range of the interaction potential. Initially, the mean distance of the particle directly below two vicinal mounds is increased, indicated by its lighter color in the first image of Figure 4. In the second image a gliding dislocation, extended about four to five monolayers, emerges. Note that this is a quite instable configuration of the system. Just due to further rearrangements of the surface, particles in deeper layers of the system are affected by this gliding dislocation and the system finally ends up with a dislocation direct on the substrate adsorbate interface. This stable configuration is shown in Figure 4, panel (3). The lateral position of such a dislocation is determined by the kinetic processes on the surface and does not show any periodicity, in contrast to the case of positive misfit.

While dislocations are built by the latter mechanism in the case of small values of negative misfit $(|\epsilon| < 6\%)$, large values of negative misfit $(|\epsilon| > 8\%)$ lead to the dislocation

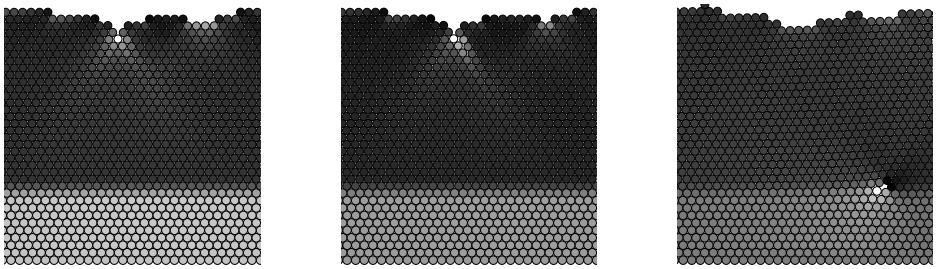

(1) *(2)* *(3)*

Figure 4: The formation of a dislocation simulated with a negative misfit $\epsilon = -5.0\%$. This sequence of snapshots shows the evolution of a section of a larger system.

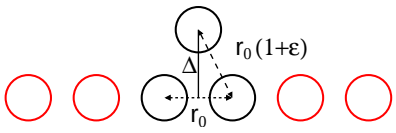

Figure 5: Illustration of the distance Δ between a particle and the underlying compressed layer. The lateral distance is the equilibrium r_0 distance of the substrate.

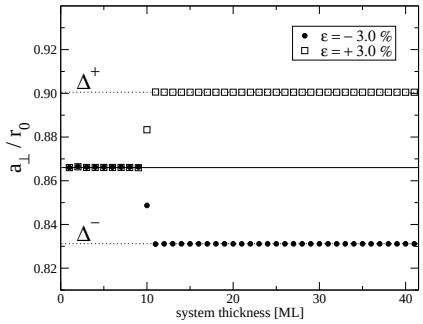

Figure 6: Development of the vertical lattice spacing with shift to $a_\perp = \Delta^+$ for positive misfit $\epsilon = +3.0\%$ and to $a_\perp = \Delta^-$ for negative misfit $\epsilon = -3.0\%$. The substrate consists of the first ten layers of the system.

formation right at the substrate adsorbate interface as discussed above. For values in between one can observe both mechanisms at different sections of the system. Consequently, the type of the dislocation depends on the surface kinetics.

3.2 Behavior of the lattice spacings

In pseudomorphic growth the adsorbate grows coherently with the lateral lattice spacing of the substrate. Due to this compression of the adsorbate film in lateral direction, the vertical lattice spacing is shifted to higher values in order to reach the equilibrium distance given by its potential. Figure 5 illustrates the expected distance Δ between two adsorbate layers. While the lateral distance r_0 is the lattice constant of the substrate, the preferred distance of two particles of different layers is $r_0\,(1+\epsilon)$. This leads to a vertical lattice spacing

$$\Delta = r_0 \sqrt{\epsilon^2 + 2\epsilon + \frac{3}{4}}. \tag{5}$$

This calculated shift can be observed in our simulation as well. To this end, some layers of adsorbate material are grown pseudomorphically on a system consisting of ten substrate monolayers. The system size was set $L = 100$ which is sufficient for this comparison. Figure 6 compares the value calculated according to Equation (5) with a single simulation for negative and positive misfit. Here $a_\perp$ describes the vertical lattice spacing between two subsequent layers in units of the equilibrium distance r_0 of the substrate.

In the simulation the vertical lattice spacing is calculated by taking the mean vertical distance of each particle to its closest neighbors in the next layer at the given thickness.

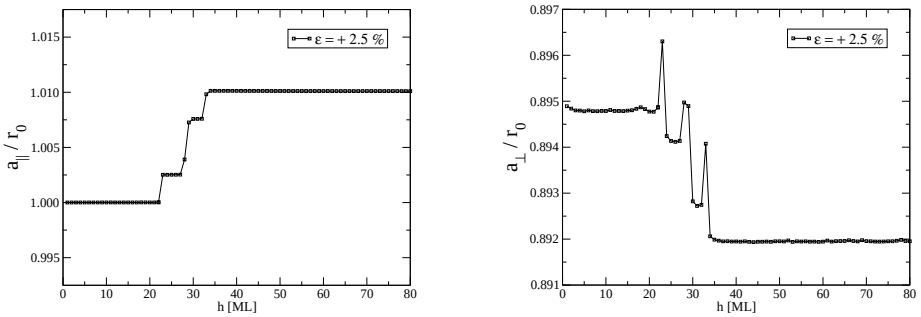

Figure 7: Development of the lateral lattice spacing $a_{\|}$ and the vertical lattice spacing $a_{\perp}$ as a function of the adsorbate film thickness h for positive misfit $\epsilon = +2.5\%$ and a system size $L = 400$. The data results from a single simulation.

In this case only particles of one single layer close to the surface are taken into account. Accordingly, the lateral lattice spacing is the mean distance of each particle of this layer to its next neighbors in the same layer. As expected, here the curves for positive and negative misfit essentially coincide. Only the top layer of the ten substrate layers is shifted as a consequence of the interaction with the adsorbate. The adsorbate then grows coherently with the vertical lattice spacing $a_{\perp} = \Delta^{+}$ in the case of positive and $a_{\perp} = \Delta^{-}$ in the case of negative misfit.

At the critical thickness the system starts to release the strain by introducing misfit dislocations. For positive misfit the number of particles in one monolayer is reduced and the mean lateral distance increased. Therefore the shift of the lateral lattice spacing is reduced and the adsorbate approaches its relaxed undisturbed bulk structure. Figure 7 displays the development of the vertical and the lateral lattice spacings for a single system of the size $L = 400$. The determination of the lattice spacing was always done during the growth simulation with downhill funneling and the displayed values show the lattice spacings close to the surface as a function of the adsorbate height. The value of each single shift which is caused by one dislocation depends on the system size as it is averaged over all particles in one layer.

The increased value of the vertical lattice spacing $a_{\perp}$ right before the sudden descent can be explained by the particles forming the dislocation. Here, two adsorbate particles of two successive layers have the same lateral position which results in an additional shift to a local vertical distance $\tilde{\Delta} = r_0\,(1 + \epsilon) > \Delta$. The concurrent appearance of several dislocations at the critical adsorbate film thickness can be seen in the curves as close successive jumps. A section of this simulated surface is shown in Figure 8.

In experimental studies it has become possible to measure the vertical lattice spacings averaged over whole adsorbate film during MBE growth [14] for systems with positive misfit. In the simulation the average vertical lattice spacing $\overline{a}_{\perp}$ is obtained by calculating the mean vertical distance of all adsorbate particles to their closest neighbors of the next layer, in contrast to the vertical lattice spacing $a_{\perp}$, where only particles of one single layer are considered. Figure 9 displays this average vertical lattice spacing $\overline{a}_{\perp}$ for the same single simulation discussed above. A qualitative comparison of the development of $\overline{a}_{\perp}$ measured in experiment and obtained in the simulations is displayed in Figure 10 which demonstrates the qualitative agreement of our results with experimental findings. In the pseudomorphic growth $\overline{a}_{\perp}$ keeps constant, which can be identified as the plateau in the beginning of the growth. An occurring dislocation does not affect the mean particle distances of the already grown adsorbate film in a significant way. Since $\overline{a}_{\perp}$ is averaged over the whole film it decreases slowly towards the undisturbed bulk value. As discussed in the previous section, for small negative misfits, dislocations formed at the surface glide down immediately to the substrate adsorbate interface. Therefore the whole adsorbate film is affected and a sudden

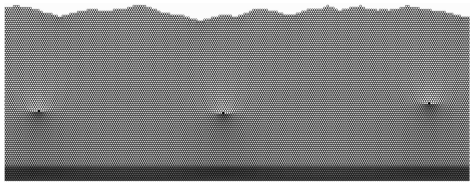

Figure 8: Section of the same system as in Figure 7 showing three dislocations. The first eight bottom layers represent the substrate.

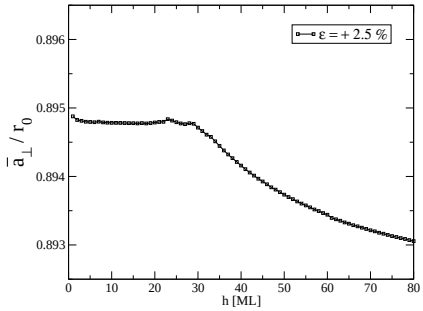

Figure 9: Development of the average vertical lattice spacing $\overline{a}_\perp$ as a function of the adsorbate film thickness h. The data results from the same single simulation shown in Figures 7 and 8.

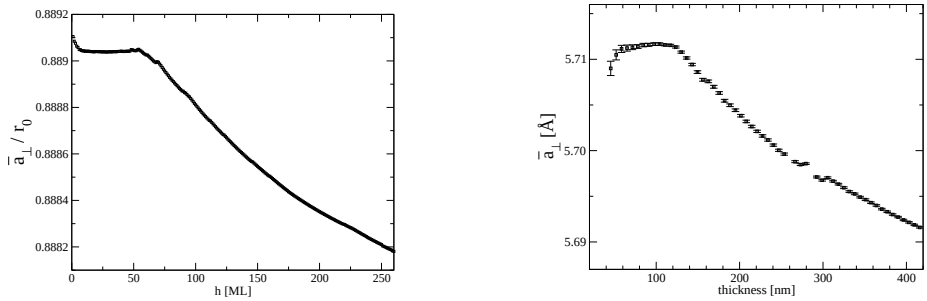

Figure 10: Development of the average vertical lattice spacing $\overline{a}_\perp$ as a function of the adsorbate film thickness. The left curve results from KMC simulation with a misfit $\epsilon = +2.0\%$, averaged over ten independent runs, the right shows experimental data of a ZnSe/GaAs system ($\epsilon \approx 0.31\%$) [14].

change of $\overline{a}_\perp$ can be expected. This expectation is confirmed by the simulation and shown in Figure 11. Every jump in the curve refers to such a gliding dislocation.

4 Influence of buried dislocations

After a dislocation is formed more and more adsorbate material is deposited and the dislocations are totally overgrown. But these buried dislocations still have influence on the subsequent growth. To study this influence on a quantitative level, we removed all particles of a grown system down to a certain film height above the dislocations. In the vicinity of its lateral position the dislocation has mainly a repulsive influence on diffusing adatoms on the surface: The modulation of the potential energy surface, see Figure 12, is such that transition state energies for particle hops toward the dislocation increase. Only right above the dislocation and, in this example situation, at the left and right neighbor sites, the transition state energy is lowered. Figure 13 shows the diffusion barrier for particle jumps to the right in the vicinity of the buried dislocation. The closer a particle approaches the lateral position of the dislocation, the higher is the necessary activation energy.

The converse effect arises if the particle moves away from the dislocation. As a consequence, the particles tend to move away from the dislocation. Only a small range directly above the dislocation is attractive for diffusing particles. Note that the modulation of the diffusion barrier depends on the thickness of the adsorbate film above the dislocation. In

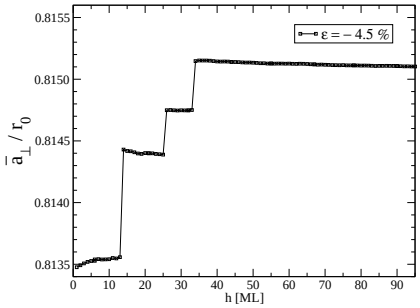

Figure 11: Development of the average vertical lattice spacing $\overline{a}_\perp$ as a function of the adsorbate film thickness. The misfit is $\epsilon = -4.5\%$ and the system size L=400.

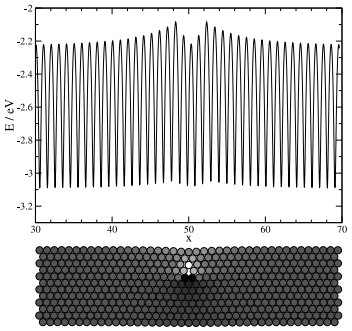

Figure 12: Potential energy surface of an adatom moving along the surface. The corresponding section of a flattened system with misfit $\epsilon = +2.5\%$ shows the detail position of its dislocation.

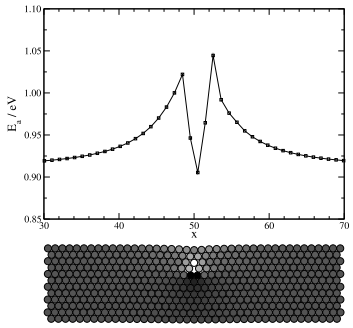

Figure 13: Diffusion barrier for particle jumps to the right at the lateral position x. The corresponding section of a flattened system with misfit $\epsilon = +2.5\%$ shows the detail position of its dislocation.

Figure 14 the diffusion barrier for jumps to the right neighboring site is compared for several adsorbate film heights. Firstly, we observe that the intensity of the modulation caused by the dislocation decreases with increasing film thickness. Secondly, the attractive range direct above the dislocation increases with the film thickness.

In systems with higher misfit normally several dislocations emerge at the critical height and therefore a diffusing particle is influenced by every dislocation in its environment. To analyze the interplay of these dislocations, a system with a misfit of $\epsilon = +5\%$ is grown and flattened at different adsorbate thicknesses. As one can see in Figure 15, in the case of positive misfit the initial repulsive character of a single dislocation changes after few layers of adsorbate. The superposition of the influence of all dislocations lead to a diffusion bias towards the lateral positions of the dislocations. The figure shows a section of a larger system with dislocations formed directly on the substrate due to the high value of misfit.

The opposite behavior can be seen for negative misfit, as shown in Figure 16. Few layers above the substrate the particles preferably diffuse to lateral positions between the dislocations that are again located directly on the substrate.

For low particle fluxes and low temperatures the modulation of the diffusion barriers caused by the buried dislocations dominates the lateral position of growing mounds. This effect can be seen in the simulation if one grows adsorbate material on an initially flattened surface. Here, the temperature is set to $T = 340\,K$ and the flux is set to $F = 1.0 \times 10^{-5}\,MLs^{-1}$. Figure 17 displays the resulting surface when growing on a flattened surface with buried dislocations for the case of negative and positive misfit. While for negative

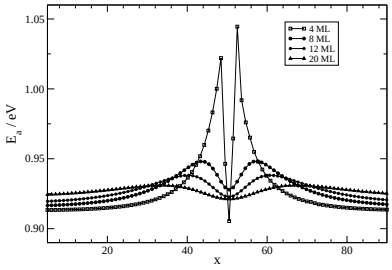

Figure 14: Activation energy for diffusion steps to the next right neighboring site on a flattened surface in different heights above the dislocation at $x = 50$. The misfit of the system is $\epsilon = +2.5\%$

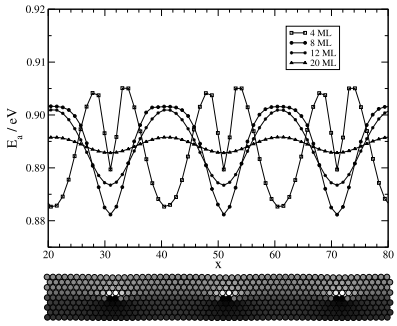

Figure 15: Activation energy for diffusion steps to the next right neighboring site on a flattened surface for different values of the adsorbate film thickness. The misfit of the system is $\epsilon = +5.0\%$

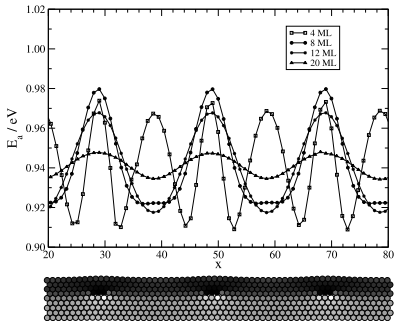

Figure 16: Activation energy for diffusion steps to the next right neighboring site on a flattened surface for different values of the adsorbate film thickness. The misfit of the system is $\epsilon = -8.0\%$

misfit the mounds are formed between the lateral positions of the dislocations, for positive misfit they appear directly above the dislocations.

Apart from statistical fluctuations this correlation between the position of the dislocations and the grown mounds is clearly apparent in our simulations.

5 Summary

Heteroepitaxial growth is investigated by numerical simulations. We use an off-lattice model with classical pair-interactions that allows for continuous particle positions. Despite the restriction to (1+1)-dimensional growth, we observe complex phenomena which can be compared with experiments and give qualitative insights into heteroepitaxial growth. Since the substrate has a different lattice spacing than the adsorbate material, a growing adsorbate film will develop strain which can be relaxed by misfit dislocations. We discuss different mechanisms of the formation of such misfit dislocations. In the initial phase one observes a pseudomorphic growth up to a critical thickness of the adsorbate film. We show that the formation of dislocations depends strongly on the sign of the misfit. While for positive misfit the dislocations keep their vertical positions, in the case of small values of negative misfit the dislocations formed at the surface glide down to the substrate adsorbate interface.

The dislocations affect the vertical and the lateral lattice spacings of the system. The average vertical lattice spacing continuously approaches the undisturbed bulk value when the misfit is positive. This observation is in qualitative agreement with experimental data. For negative misfit, however, the average vertical lattice spacing approaches the bulk ad-

$\epsilon = +5.0\%$ $\epsilon = -8.0\%$

Figure 17: Growth on a flattened surface with buried dislocations on a system with 10 ML substrate and 7 ML adsorbate. The section of a larger system shows the surface with 23 ML of adsorbate.

sorbate value in a discontinuous manner, since dislocations glide down to the substrate immediately after their formation.

The dislocations also affect the subsequent growth of the film. We observe a clear correlation between the lateral positions of buried dislocations and the positions of mounds grown on the surface. The correlation depends decisively on the sign of the misfit. For positive misfit, mounds are preferentially formed directly above buried dislocations whereas for negative misfit, mounds grow between the lateral positions of the dislocations.

Acknowledgement
This work was supported by Deutsche Forschungsgemeinschaft through a research grant and Sonderforschungsbereich 410.

References

[1] F. Much, M. Ahr, M. Biehl and W. Kinzel, Europhys. Lett., **56 (6)**, 791 (2001).

[2] F. Much, M. Ahr, M. Biehl and W. Kinzel, Comput. Phys. Commun., **147**, 226 (2002).

[3] A. Schindler, Dissertation, Universität Duisburg, (1999).

[4] D.A. Faux, G. Gaynor, C.L. Carson, C.K. Hall and J. Bernholc, Phys. Rev. B,**42**,2914(1990).

[5] W.M. Plotz, K. Hingerl and H. Sitter, Phys. Rev. B ,**45**, 12122 (1992).

[6] J. Kew, M.R. Wilby and D.D. Vvdensky, J. Cryst. Growth, **127**, 508 (1993).

[7] F. Much and M. Biehl, Europhys. Lett., **63 (1)**, 14 (2003).

[8] A. Pimpinelli and J. Villain, Physics of crystal growth, Cambridge University Press (1998).

[9] G.T. Barkema and N. Mousseau, Phys. Rev. E., **57 (2)**,2419 (1998).

[10] M. Schroeder, D.E. Wolf, Surf. Sci., **375**, 129 (1997).

[11] W.H. Press, S.A. Teukolsky and W.T. Vetterling, Numerical Recipes in C: The Art of Scientific Computing, Cambridge University Press, pp. 420 - 425 (1993).

[12] R.L. Schwoebel and E. J. Shipsey, J. Appl. Phys., **37**,3682 (1966).

[13] M. Biehl, F. Much, C. Vey, in: Multiscale Modeling in Epitaxial Growth, ed. A. Vogt, International Series of Numerical Mathematic, **149** (Birkhaeuser 2005),pp. 41 - 57.

[14] A. S. Bader, W. Faschinger, C. Schumacher, J. Geurts, and L. W. Molenkamp, Appl. Phys. Lett.,**82**,4684(2003).